THE JOURNAL OF PHYSICAL CHEMISTRY C
A JOURNAL OF THE AMERICAN CHEMICAL SOCIETY

pubs.acs.org/JPCC

Article

# Revealing the Variation of Photodetectivity in $MAPbI_3$ and $MAPb(I_{0.88}Br_{0.12})_3$ Single Crystal Based Photodetectors Under Electrical Poling-Induced Polarization

Apurba Mahapatra,* Rohit D. Chavan, Mohammad Mahdi Tavakoli, Pawan Kumar, Abul Kalam, Daniel Prochowicz,* and Pankaj Yadav

Cite This: *J. Phys. Chem. C* 2022, 126, 13458−13466

Read Online

ACCESS | Metrics & More | Article Recommendations | Supporting Information

**ABSTRACT:** The use of electrical poling to induce polarization potential has been found to increase the photocurrent ($I_{light}$) in hybrid perovskite-based devices; however, the origin of this process has not been fully understood. Here, we study the effect of electrical poling on the photodetection properties of self-powered photodetectors (PDs) based on halide perovskites in two different phase structures (i.e., tetragonal and cubic). Specifically, extensive investigations are performed on the $MAPbI_3$ (tetragonal) and $MAPb(I_{0.88}Br_{0.12})_3$ (cubic) single crystals (SCs). Our characterization results revealed that the $I_{light}$ has increased by 2-fold during forward poling and decreased during reverse poling in both PDs. The improved $I_{light}$ is caused by polarization induced ion migration, which builds remanent potential due to ion accumulation near metal electrodes. The effect of this polarization was found to be greater in $MAPbI_3$ PD as compared to $MAPb(I_{0.88}Br_{0.12})_3$ PD, which influences the interface band bending and reduces Schottky barrier height (SBH). This study highlights that the modification of SBH, which describes the potential energy barrier for electrons formed at a metal−semiconductor junction, can tune the photocurrent and response time of PDs.

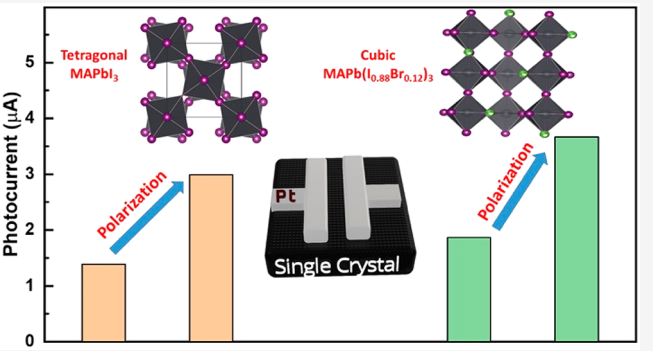


## 1. INTRODUCTION

Since the first application of methylammonium lead iodide ($MAPbI_3$) as a photovoltaic absorber layer in 2009,[1] lead halide perovskites (LHPs) have been largely studied as semiconducting materials due to their high absorption coefficients, long carrier diffusion lengths, and high carrier mobility.[2,3] In addition, the ease of fabrication and adjustable bandgap of LHPs make them great candidates for many technological applications, including photodetectors,[4] single and multijunction solar cells,[5−7] light-emitting diodes,[8,9] and transistors.[10] However, low operational stability and polarization phenomenon of perovskite materials affect the charge transport and recombination during the operation of devices. These issues mainly stem from mobile ions and vacancies, which are caused by the loosely bonded crystal structure of LHPs.[11] Moreover, ion migration within perovskite solar cells (PSCs) under an external electric field can lead to the photocurrent ($I_{light}$) hysteresis,[11,12] slow photoresponses,[13,14] photoinduced phase separation,[15,16] and low device stability.[17] The majority of perovskite-based devices are based on polycrystalline films, which may suffer severe instabilities due to morphological disorder at grain boundaries, ion migration, and surface degradation under ambient conditions.[18−20] Recently, extensive efforts have been devoted to developing LHPs in the form of single crystals (SCs) due to their higher carrier diffusion length, longer lifetime, and a lower trap state density than the corresponding polycrystalline counterparts.[21,22] Moreover, the lack of morphological disorder at grain boundaries in SCs reduces the recombination pathways of the excited carriers. Thus, high-quality perovskite SCs-based devices show huge promise for the next generation of photodetection such as optical communication, sensing, and imaging applications.[21,23]

It is reported that mobile species (ions and vacancies) can migrate through the crystal structure of LHPs and accumulate near an electrode under applied bias and/or device potential.[24−27] These accumulated species reduce the effective electric field and affect the charge extraction and transport properties within the perovskite devices.[24,28] In the majority of recent studies, a high voltage was applied for poling, which not

Received: May 31, 2022
Revised: July 19, 2022
Published: July 28, 2022

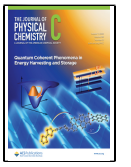

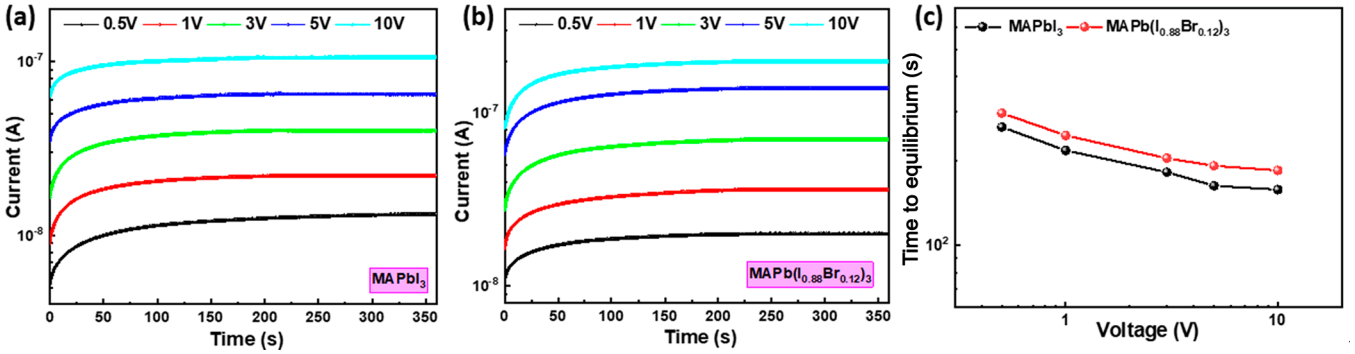


**Figure 1.** Time-dependent dark current at different voltages ranging from 0.5 to 10 V for (a) $MAPbI_3$ and (b) $MAPb(I_{0.88}Br_{0.12})_3$ SC-based PDs. (c) Time taken for achieving steady-state current as a function of applied bias for both SC-based PDs.

only induces ion migration inside the perovskite device but also triggers the degradation of the perovskite layer.[25,29,30] For example, Leijtens et al. used a high electric field (>60 V) to polarize the perovskite film and demonstrated its structural degradation.[24] Notably, electrical poling has been performed primarily on PSCs due to their big success in improving power conversion efficiency[31] with much larger open-circuit voltage[32] and less photocurrent ($I_{light}$) hysteresis.[29] Moreover, PSCs and most perovskite-based photodetectors (PDs) contain carrier transport layers that predetermine the direction of photo-excitons. To expand the application of poling on LHP based devices, it is vital to understand the effect of electrical poling and poling-induced ion migration on the electronic properties of perovskites-based devices without any additional layer. In this context, perovskite-based PDs with planar architecture is an ideal device to study the poling effect due to their simple structure, containing only the absorber material and metal electrodes as electrical contacts. Moreover, planar PDs can form a Schottky junction between the perovskite semiconductor and metal electrodes.[33,34] The performance of these PDs mainly depends on the quality of thin films or SCs[22,34] and the Schottky barrier height ($\Phi_{SB}$, SBH) between the metal and semiconductor,[35,36] which describes the energy barrier for the charge carriers to pass through the contact. For example, Nea et al. applied the strain to create a piezoelectric potential on the $MAPbI_3$ thin film-based PDs and changed the SBH, which affects the $I_{light}$.[37] In another work, Lan et al. used electrical poling to promote the polarization potential of $MAPbBr_3$ based PDs, which enhanced the $I_{light}$ and improved the response time.[13] The redistribution of mobile ions (ion migration) under external bias can create n-type and p-type regions at grain boundaries and/or the metal/semiconductor interface leading to the formation of an internal electric field and change in the SBH. A recent study by Lin et al. revealed that there is a different order of ion migration and $MA^+$ dipole rotation in $MAPbX_3$ (X = I, Br, Cl), which depends on the activation energy and lattice structure.[38] However, the systematic understanding of the poling-induced ion migration in single crystalline perovskite-based PDs is still lacking.

In this work, we study the effect of external electrical poling on the photodetection properties of SC PDs based on $MAPbI_3$ (tetragonal) and $MAPb(I_{0.88}Br_{0.12})_3$ (cubic) perovskite compositions. First, we investigate the electric-field-induced ion migration using time-dependent dark current under variable biases. We found that $MAPb(I_{0.88}Br_{0.12})_3$ SCs require a higher time to achieve saturation current under applied biases than $MAPbI_3$ SCs due to their slower ion migration process. Next, we induced polarization inside the SC PDs under dark conditions using a continuous and stepwise external electric bias. These experiments showed that the external field accumulates mobile ions near the electrode forming a remanent field, which affects the photodetectivity of the PDs. To further understand the effect of positive and negative electrical poling, we also studied the photoresponses of our PDs under ±0.5 V operating voltage and after electric poling with ±5 V stepwise external electric bias. The change in photocurrent of both SC-based PDs, caused by the ion accumulation, modifies the SBH between the metal electrodes and perovskite SC surface. As a result, our PDs showed tunable photocurrent and response time depending on the direction of the applied electric field.

## 2. EXPERIMENTAL SECTION

**Synthesis and Characterization of $MAPbI_3$ and $MAPb(I_{0.88}Br_{0.12})_3$ SCs.** $MAPbI_3$ and $MAPb(I_{0.88}Br_{0.12})_3$ SCs used in this study were synthesized using the inverse temperature crystallization (ITC) method. A 1 M $MAPbI_3$ solution and a 1 M $MAPb(I_{0.88}Br_{0.12})_3$ solution were prepared by adjusting the portion of lead(II) iodide ($PbI_2$), lead(II) bromide ($PbBr_2$), and methylammonium iodide (MAI) in gamma-butyrolactone (GBL). The mixtures were stirred for 24 h at 60 °C. Next, all the solutions were filtered using a 0.24 $\mu$m PTFE filter. A 2mL aliquot of each filtered transparent solution was sealed in bottles and kept at 110 °C for 4 h in an oil bath, which resulted in the growth of large SCs. The crystals were washed with acetone 2−3 times and then dried at 100 °C for 20 min. Both the SCs were ground, and powder X-ray diffraction (pXRD) patterns were recorded with a Rigaku Ultima IV with Cu K$\alpha$ radiation ($\lambda$= 1.5406 Å) over a 2$\theta$ range of 10° to 50° without rotating the sample at room temperature. To perform time-dependent EIS measurements characteristics, thin layers of silver (Acheson Silver. Product no: G 3692) were deposited on both sides of $MAPbI_3$ SC. Time-dependent EIS measurements were performed using a potentiostat Autolab (Metrohm Autolab) equipped with a frequency response analyzer.

**Fabrication and Characterization of Photodetectors.** Platinum (Pt) electrodes were deposited by thermal evaporation on the (100) facets of the SCs with a channel of 500 $\mu$m length by 2 mm width. The schematic diagram of the PDs is shown in Figure S2. The photocurrents of the both PDs were studied using a potentiostat Autolab (Metrohm Autolab) and an LCR meter with a white LED light source in the open


https://doi.org/10.1021/acs.jpcc.2c03735
J. Phys. Chem. C 2022, 126, 13458−13466

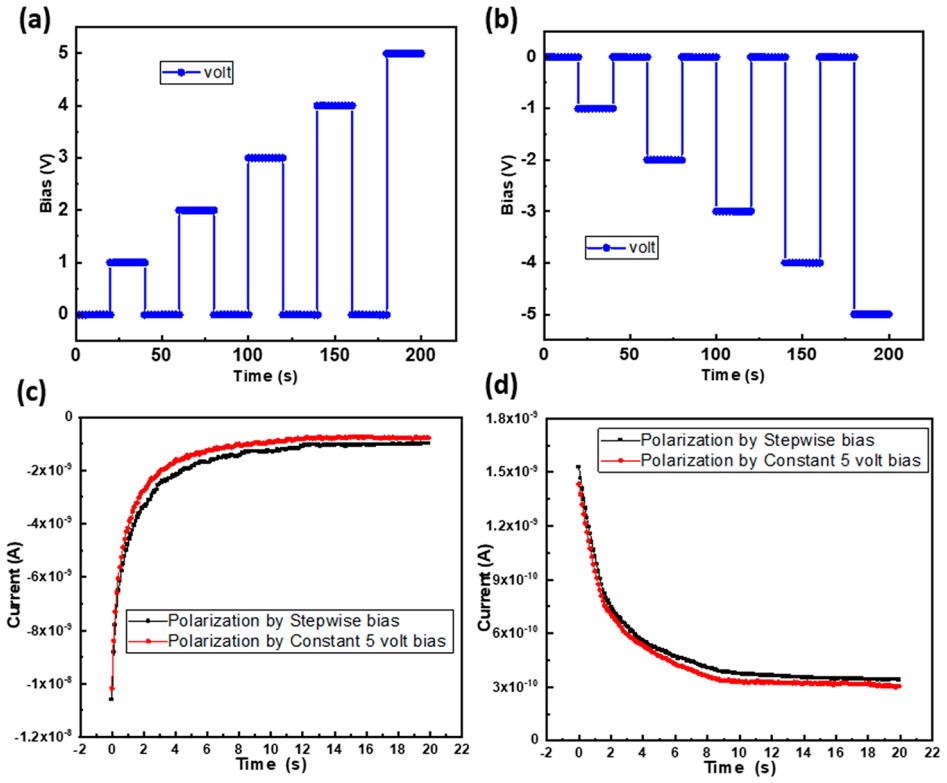


**Figure 2.** (a,b) Voltage−time ($V$−$t$) curves of the applied pulsed stepwise bias to induce remanent field for $MAPbI_3$ SC based PD. (c) Remanent negative current produced by +5 V pulsed stepwise bias and constant bias for $MAPbI_3$ SC based PD. (d) Remanent positive current produced by −5 V pulsed stepwise bias and constant bias for $MAPbI_3$ SC based PD.

air. For polarization of both the PDs, potentiostat Autolab (Metrohm Autolab) with a modified program was used.

## 3. RESULTS AND DISCUSSION

**3.1. Time-Dependent Dark Current.** While $MAPbI_3$ perovskite exhibits a tetragonal crystal structure, the mixed halide perovskite alloy with the minimum 12% Br content, that is, $MAPb(I_{0.88}Br_{0.12})_3$ has a cubic structure at room temperature.[34] Thus, these compounds were selected to act as a convenient platform for studying the effect of external electrical poling on the photodetection properties of SC PDs depending on the perovskite phase structure (i.e., tetragonal and cubic). Both compounds in the form of SCs were synthesized using the inverse temperature crystallization (ITC) method, and their pure phase formation was confirmed by X-ray diffraction (XRD) (Figure S1). Figure S2 shows the Pt−SC−Pt lateral electrode configuration structure, which was used in this study (for details of crystal growth and device fabrication see Experimental Section). First, we measure the time-dependent dark current under a variable potential difference to investigate the charge dynamics in our PDs. Figure 1 panels a and b show the time-dependent dark current at a voltage ranging from 0.5 to 10 V for the $MAPbI_3$ and $MAPb(I_{0.88}Br_{0.12})_3$ SC based PDs, respectively. Both PDs show a lower current at the starting time, which increases exponentially with the time and reaches saturation at a higher value of time. At the beginning, electronic conductivity dominates under an applied potential due to fast response of electrons and holes.[38] Our previous studies on the perovskite SCs demonstrated that ions need a higher time to migrate than electrons and it can vary under various applied voltages.[39,40] Therefore, ion migration under an applied electric field dominates the dark current, and its contribution increases at the higher time region.[38] The dark currents as a function of applied potential at different times for both PDs are summarized in Figure S3. It can be observed that the current at the ending time (300 s) is significantly larger than that at the starting time (0 s) due to the contribution of mobile ions movement to the current, which significantly increases with time and intensifies under a higher applied bias. The difference between starting current (0 s ($I_0$)) and saturated current ($I_s$) for the $MAPbI_3$ SC is higher than that found in the $MAPb(I_{0.88}Br_{0.12})_3$ SC (Figure S3a,b) indicating a higher contribution of ion migration to the current in $MAPbI_3$ SC based PD. Recently, we reported that the phase transition from tetragonal to cubic ($pm\bar{3}m$) phase can occur when 12% Br is introduced into the crystal structure of $MAPbI_3$.[34] This phase transition also leads to the reduction in lattice constant, lower trap density, higher activation energy, and higher carrier mobility. Due to a higher activation energy for the ion migration, we can expect a lower current difference between starting (0 s) and saturated currents under the external bias in the $MAPb(I_{0.88}Br_{0.12})_3$ SC. Figure 1c compares the time to reach steady-state as a function of applied bias for both samples. As seen, the $MAPb(I_{0.88}Br_{0.12})_3$ SC takes a higher time to saturate the current for every applied bias indicating its slower ion migration, which restricts the cation dynamic and movement of mobile ions.

**3.2. Polarization Induced Remanent Current.** Recent studies demonstrated that there is a strong effect of polarization on the photodetection of LHP-based PDs.[13,34,37] Moreover, Liu et al. revealed the existence of a remanent field inside LHPs due to the bias-induced ion accumulation, which was produced by a pulsed stepwise electric wave.[41] In this part, we used a constant electric field and pulsed stepwise electric


https://doi.org/10.1021/acs.jpcc.2c03735
J. Phys. Chem. C 2022, 126, 13458−13466

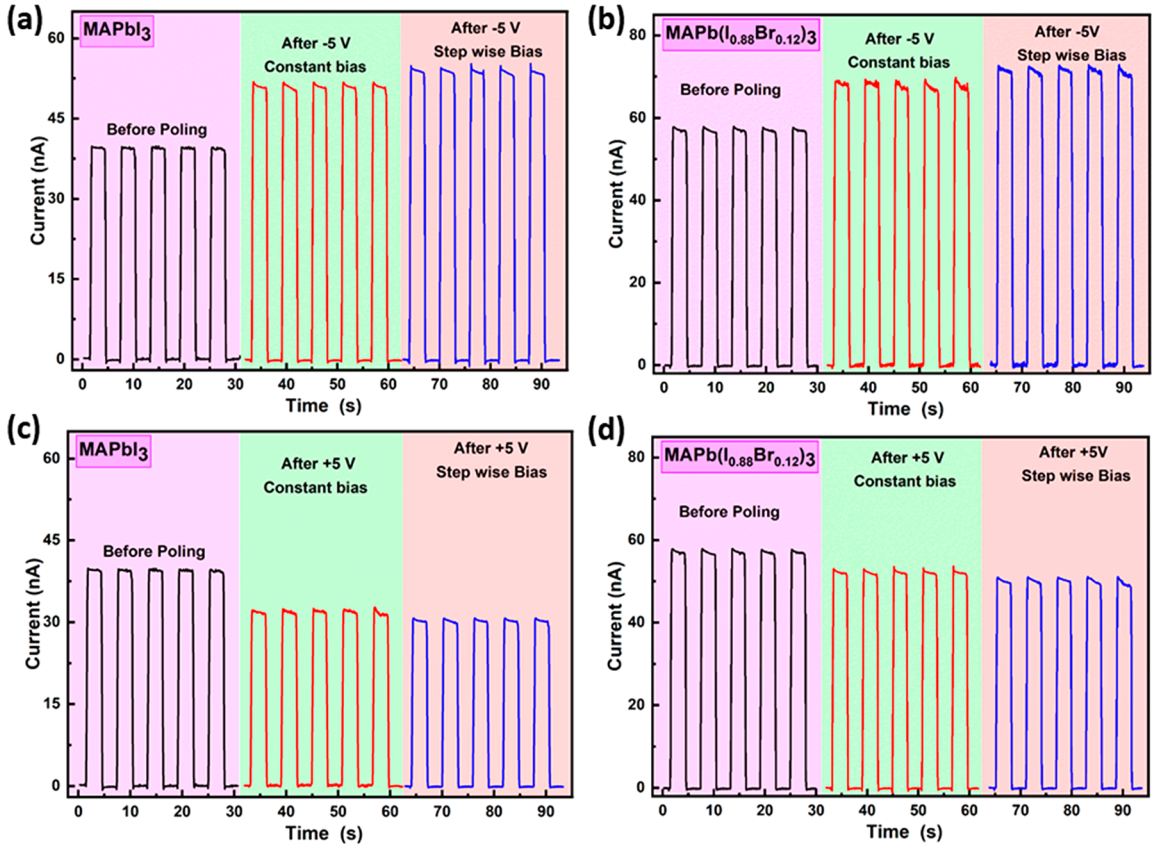


**Figure 3.** Current−time ($I$−$t$) characteristics of (a) $MAPbI_3$ and (b) $MAPb(I_{0.88}Br_{0.12})_3$ SC-based self-powered PDs before and after −5 V constant bias as well as under a pulsed stepwise bias (up to −5 V). Current−time ($I$−$t$) characteristics of (c) $MAPbI_3$ and (d) $MAPb(I_{0.88}Br_{0.12})_3$ SCs based self-powered PDs before and after +5 V constant bias as well as under a pulsed stepwise bias (up to −5 V).

wave to find a fast and effective way to create higher polarization inside the SC-based PDs. Specifically, a ±5 V constant bias for 200 s and pulsed stepwise bias with 20-s pulse duration (total 200 s) were applied on the $MAPbI_3$ SC-based PD to create a remanent field (Figure 2a,b). A low electric field was used to create polarization due to the prone of LHPs to degrade under high electric fields.[24] We observed that the $I$−$t$ curve under dark after +5 V constant bias and pulsed stepwise bias does not reach 0 A (Figure 2c). Thus, the negative off-field dark current after polarization by both applied methods suggests accumulation of the opposite mobile ions nearby the electrode. A higher remanent negative current is generated after pulsed stepwise bias than that of constant bias. This indicates a higher degree of mobile ion accumulation nearby the electrode interface. A similar effect is also recorded for −5 V constant bias and pulsed stepwise bias on the $MAPbI_3$ SC-based PDs. But the order of remanent current after polarization is less than that of remanent current after +5 V bias (Figure 2d). A similar effect of polarization is also observed for the $MAPb(I_{0.88}Br_{0.12})_3$ SC-based PD, as shown in Figure S4. The reason for the observed difference in remanent currents will be discussed in the next section.

To get better understanding of the remanent field, induced by polarization, we performed time dependent electrochemical impedance spectroscopy (EIS). We did EIS measurements as a function of time in the frequency range from 1 MHz to 100 mHz at an AC perturbation voltage of 25 mV and under dark conditions. Figure S5 shows the EIS Nyquist spectra of the $MAPbI_3$ SC before and after polarization. It is well-established that the low frequency region of impedance is attributed to the ion motion/ionic polarization, while the high-frequency part of the impedance response relates to the electronic bulk conductivity.[26,39,40,42] We observed that the resistance related to the high-frequency part of the impedance increases after the polarization and decreases with time due to the ion redistribution. This behavior can be attributed to the change of electronic doping of the perovskite bulk by the dynamic mobile ions. The drift of cation vacancies fill the space or defects, makes material more intrinsic-like, and increases the resistance related to the high-frequency part.[26,42] Here, such change of the high-frequency part of the impedance due to polarization is not observed. Instead, we observe a change in the low frequency region of impedance after polarization, which is almost constant up to 6 h. Therefore, the change in the impedance after polarization comes from the redistribution and accumulation of ions, which creates the remanent field. The low frequency impedance changes rapidly with time after 15 h of polarization and almost back to the initial level after 24 h. Therefore, the effect of polarization is reduced with increasing the time and is almost automatically removed after 24 h of polarization.

**3.3. Effect of Polarization in Self-Powered Conditions on PDs.** In case of the planar PD, an external electric bias is usually used to enhance the photocurrent ($I_{light}$) and the direction of the $I_{light}$ can be tuned by changing the direction of the applied bias.[13] Before the poling process, the photocurrent of $MAPbI_3$ and $MAPb(I_{0.88}Br_{0.12})_3$ SC-based PDs under different light intensities was investigated using a white LED at 1 V operating voltage (Figure S6). The photocurrents of both PDs displayed a good linear dependency with the


https://doi.org/10.1021/acs.jpcc.2c03735
J. Phys. Chem. C 2022, 126, 13458−13466

incident light intensity. The $I_{light}$ increases with increasing the light intensity due to the increment of photoexcited carriers. The $MAPb(I_{0.88}Br_{0.12})_3$ PD shows higher $I_{light}$ due to their lower trap density and higher carrier mobility than $MAPbI_3$ SCs, which was observed in our recent study.[34] The dark currents of the $MAPbI_3$ and $MAPb(I_{0.88}Br_{0.12})_3$ SC-based PDs are shown in Figure S7. We observed an asymmetric dark current response for both $MAPbI_3$ (0.9 $\mu$A at 3 V and −1.09 $\mu$A at −3 V) and $MAPb(I_{0.88}Br_{0.12})_3$ (1.11 $\mu$A at 3 V and −1.28 $\mu$A at −3 V) based PDs. Moreover, the photocurrents of both PDs at 10 mW/cm$^2$ white light illumination increases with increasing applied bias due to more efficient charge extraction under a higher bias as shown in Figure S8a,b. Notably, the $I_{light}$ generated under positive +3 V applied bias was found to be lower than that generated with the −3 V negative bias for both PDs. These asymmetric results (asymmetric dark current and photocurrents) indicate the formation of an asymmetric Schottky junction between the SC surface and metal contact (Pt). Despite the symmetrical electrode structure on the SCs, our recent study showed that the lateral structured $MAPbI_3$ and $MAPb(I_xBr_{1-x})_3$ SC-based PDs show self-photodetectivity due to the asymmetric morphology of the crystal surface, which produced an asymmetric Schottky barrier height (SBH) between the two electrodes.[13,34]

To investigate the effect of polarization-induced ion migration on two differently oriented crystal structures, the electrical poling on the tetragonal $MAPbI_3$ and cubic $MAPb(I_{0.88}Br_{0.12})_3$ SC-based PDs was scrutinized. In the case of self-powered PDs, the sign of $I_{light}$ (positive or negative) depends on the electrical connection with the instrument due to the asymmetric Schottky junction. A small positive $I_{light}$ of both PDs is recorded before poling under 10 mW cm$^{-2}$ white light. Next, our PDs were polarized under both constant ±5 V external biases for 200 s and pulsed stepwise bias in the dark. The current−time ($I$−$t$) characteristics of both SC-based PDs before and after polarization are shown in Figure 3. The $I_{light}$ of both PDs decreases after poling by positive bias (polarization by +5 V continuous and stepwise bias) and increases after poling by negative bias (polarization by −5 V continuous and stepwise bias) (Table 1). As seen in Figure 3a, the $I_{light}$ increases from 39.6 nA to 51 nA (28.8%) and to 54.1 nA (36.6%) after continuous and stepwise polarization by −5 V, respectively. In turn, the $I_{light}$ for $MAPb(I_{0.88}Br_{0.12})_3$ PDs enhances from 57.8 nA to 68.3 nA (18.1%) and 71.1 nA (23%), respectively, under the same poling condition (Figure 3b). The further increased poling voltage up to 10 V shows a limited effect on the $I_{light}$ of the $MAPbI_3$ SC based PDs (Figure S9). We note that the use of polarization voltage higher than 10 V can lead to the degradation of the PDs.[13] The $I_{light}$ of $MAPbI_3$ and $MAPb(I_{0.88}Br_{0.12})_3$ SC-based PDs decreases after +5 V continuous and stepwise polarization by −5 V as shown in Figure 3 panels c and d, respectively. The effect of polarization is greater in the $MAPbI_3$ PD than that of the $MAPb(I_{0.88}Br_{0.12})_3$ PD due to its higher susceptibility to the ion migration, leading to ion accumulation near the metal electrodes. The above results confirm that electric poling could significantly affect the self-powered photodetection of the SC-based PDs.

**Table 1. Photocurrents of Self-Powered PDs (before and after Polarization)**

| | photocurrents ($I_{light}$) | |
|---|---|---|
| polarization | $MAPbI_3$ | $MAPb(I_{0.88}Br_{0.12})_3$ |
| before polarization | 39.6 nA | 57.8 nA |
| after −5 V constant bias | 51 nA (28.8%) (↑) | 68.3 nA (18.1%) (↑) |
| up to −5 V pulsed stepwise bias | 54.1 nA (36.6%) (↑) | 71.1 nA (23%) (↑) |
| after +5 V constant bias | 31.5 nA (20.4%) (↓) | 52.7 nA (8.8%) (↓) |
| up to +5 V pulsed stepwise bias | 30.2 nA (23.7%) (↓) | 50.4 nA (12.8%) (↓) |

**3.4. Effect of Polarization under Operating Voltage.** To further study the effect of forward and reverse poling on the PDs, we performed similar measurements under ±0.5 V operating voltages. The operating voltage plays a positive role in the efficient charge extraction leading to a higher $I_{light}$. In the case of the $MAPbI_3$ SC-based PD, the $I_{light}$ enhances from 1.39 $\mu$A to 2.83 $\mu$A (103.6%) after forward poling (*i.e.*, poling electric field direction and operating voltage (+0.5 V) have the same direction) and to 2.99 $\mu$A (115.1%) using +5 V continuous and stepwise polarization (Figure 4a). In turn, the $I_{light}$ of $MAPb(I_{0.88}Br_{0.12})_3$ SC-based PD increases from 1.87 $\mu$A to 3.45 $\mu$A (84.5%) and 3.67 $\mu$A (96.3%) under similar conditions (Figure 4b). This is in contrast to the self-powered photodetection results shown in Figure 3c,d, where $I_{light}$ decreases under a positive polarization field (polarization by +5 V). The $I_{light}$ of both PDs enhances by the forward poling when the direction of the external bias for poling and operating voltage were both reversed (*i.e.*, −0.5 V operating voltage and −5 V for poling), as shown in Figure 4c,d. This similar behavior was observed under self-power PD conditions (Figure 3a,b). The order of change in $I_{light}$ after polarization is much larger under operating voltage than that under self-powered PD conditions. Recently, Lan et al., demonstrated that the reverse poling (*i.e.*, the electric field direction for poling and operating voltage have opposite direction) decreases the photocurrent of hybrid perovskite PDs.[13] To check the effect of reverse poling on our PDs, we applied +5 V continuous +5 V stepwise polarization and measured the photocurrent under −0.5 V operating voltage (Figure S8, Figure 4e,f). As expected the $I_{light}$ decreases after applying reverse poling for both samples. All results are summarized in Table 2. The reason behind different enhanced abilities of $I_{light}$ under negative and positive poling biases under forward poling conditions may be attributed to the screening effect of free carriers.[43,44] It is also interesting to note that poling also affects the response time of the PDs. As shown in Table 2, the response times (especially rise time (on time)) were significantly reduced after poling. The SBH is adjusted by polarization-induced remanent potential, which causes interface band bending. As a result, photogenerated carriers separated easily due to the better band alignment between SCs and the electrode (Pt). The detailed SBH evolution is discussed in the next part.

On the basis of above results, the change in photocurrent and response time of PDs could be primarily triggered by polarization induced ion migration, which leads to ion accumulation nearby the metal electrodes. In addition, there is a possibility of ferroelectric domain,[45−47] which may also contribute to the changes of $I_{light}$ under the applied electric poling. The formation of a ferroelectric domain was found to suppress the radiative electron−hole recombination because the spontaneous polarization of ferroelectric domains helps the separation of opposite charges.[47] It was reported that the $MAPbI_3$ with a tetragonal crystal structure shows ferroelec-


https://doi.org/10.1021/acs.jpcc.2c03735
J. Phys. Chem. C 2022, 126, 13458−13466

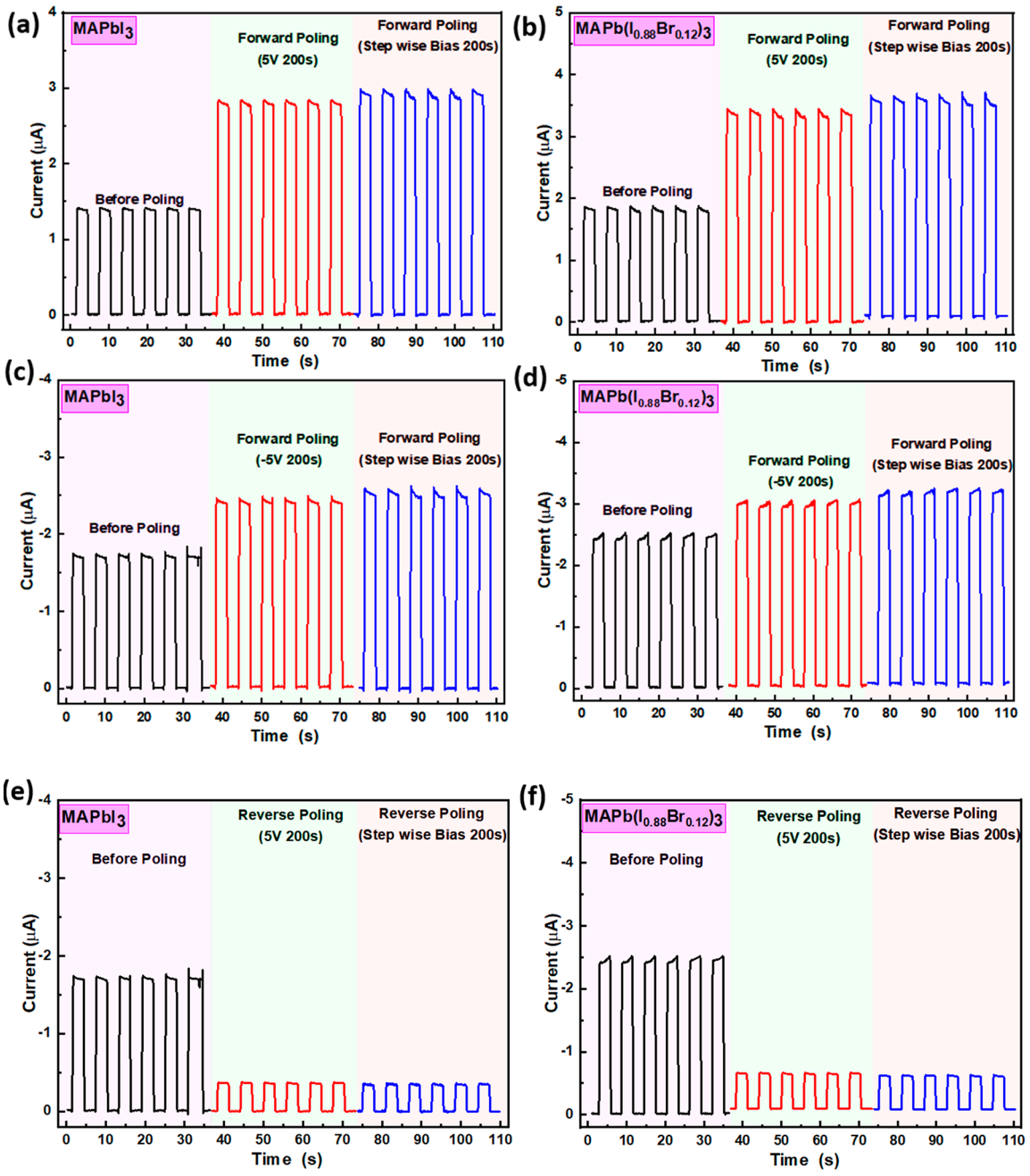


**Figure 4.** Current−time ($I$−$t$) characteristics of (a,c) $MAPbI_3$ and (b,d) $MAPb(I_{0.88}Br_{0.12})_3$ SC-based PDs before and after forward poling. Current−time ($I$−$t$) characteristics of (e) $MAPbI_3$ and (f) $MAPb(I_{0.88}Br_{0.12})_3$ SC-based PDs before and after reverse poling.

**Table 2. Photocurrents and On/Off Time of PDs under Different Polarization Conditions**

| | $MAPbI_3$ | | $MAPb(I_{0.88}Br_{0.12})_3$ | |
|---|---|---|---|---|
| polarization bias | photocurrents | on/off time (ms) | photocurrents | on/off time (ms) |
| | Operating Voltage = +0.5 V | | | |
| before polarization | 1.39 μA | 73/56 | 1.87 μA | 63/52 |
| after +5 V constant bias | 2.83 μA (103.6%) (↑) | 69/42 | 3.45 μA (84.5%) (↑) | 58/35 |
| up to +5 V pulsed stepwise bias | 2.99 μA (115.1%) (↑) | 69/40 | 3.67 μA (96.3%) (↑) | 55/32 |
| | Operating Voltage = −0.5 V | | | |
| before polarization | 1.75 μA | 75/59 | 2.51 μA | 68/51 |
| after −5 V constant bias | 2.47 μA (41.1%) (↑) | 70/48 | 3.05 μA (21.5%) (↑) | 63/42 |
| up to −5 V pulsed stepwise bias | 2.57 μA (46.9%) (↑) | 71/49 | 3.21 μA (27.9%) (↑) | 64/41 |
| after +5 V constant bias | 0.37 μA (73.5%) (↓) | 78/58 | 0.65 μA (65.2%) (↓) | 68/55 |
| up to +5 V pulsed stepwise bias | 0.35 μA (74.8%) (↓) | 79/58 | 0.61 μA (67.4%) (↓) | 68/55 |



https://doi.org/10.1021/acs.jpcc.2c03735
J. Phys. Chem. C 2022, 126, 13458−13466

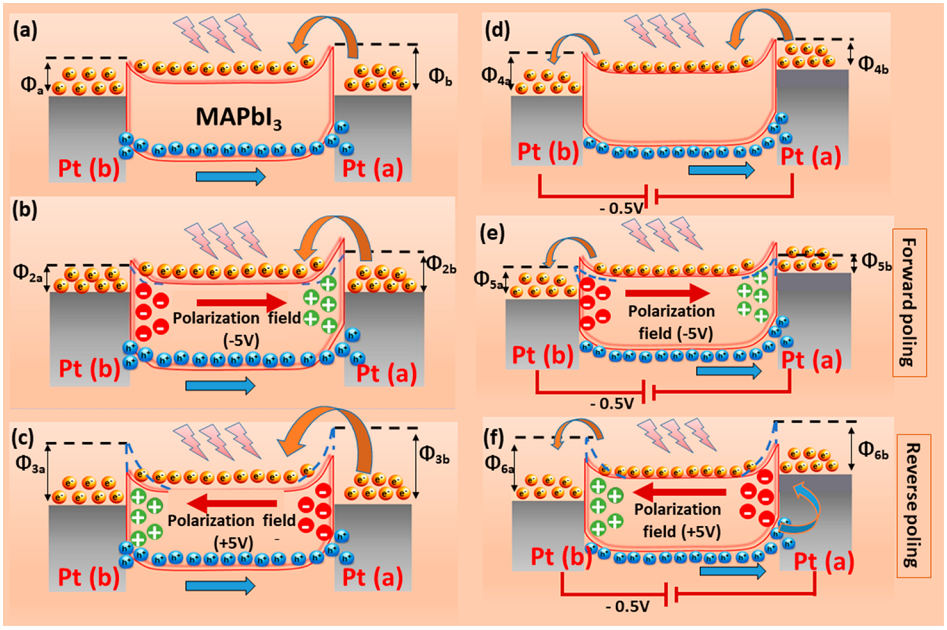


**Figure 5.** Proposed mechanism to discuss the change in photocurrent of PDs under electrical poling. Schematic illustration of band diagrams of self-powered PD during the photocurrent measurement: (a) before polarization and after polarization by (b) −5 V and (c) + 5 V. (d) Schematic illustration of band diagrams of PD during the photocurrent measurement under external operating voltage. The energy band and ions' redistribution in PD after (e) forward and (f) the reverse poling.

tricity under polarization.[45] But in the case of single crystalline $MAPbI_3$, ferroelectricity behavior can be detected only under high voltage (>50 V).[48] On the other hand, the $MAPb(I_{0.88}Br_{0.12})_3$ perovskite exhibits cubic structure at room temperature, which does not meet the criteria of crystal structure for ferroelectricity.[49] As a result, we ignore the contribution of ferroelectricity to the changes in $I_{light}$ for both PDs. Therefore, only ion accumulation might influence the interface band bending in the presence of light and help achieve a higher electrical output. Different poling effects on the photocurrent of both PDs can be discussed by the evolution of Schottky barrier height (SBH) between the Pt electrode and perovskite SC, and the presence of a remanent field. Figure 5a illustrates the photocurrent modulation in the perovskite SC-based PDs under self-powered conditions (operating voltage 0 V). There is a difference between the Fermi level between two metal electrodes (marked as Pt (a) (source) and Pt (b) (drain)) due to asymmetric morphology of the crystal surface, which produces asymmetric SBH between Pt (a) and Pt (b) electrodes. Under illumination, photogenerated electrons move to Pt (a) and holes move to Pt (b) electrodes producing photocurrent. The photocurrent strongly depends on the effective separation transport of both electrons and holes, which depends on the SBH and crystal quality. We note that $MAPb(I_{0.88}Br_{0.12})_3$ SC has lower trap density and higher bandgap than $MAPbI_3$ SC. This leads to a better SBH alignment and higher $I_{light}$. Specifically, we observed that the $I_{light}$ of both PDs enhances after −5 V polarization. During this poling, the cations (*i.e.*, $MA^+$ and $Pb^{2+}$) move along the direction of applied bias (toward Pt (a)), while the anions (*i.e.*, $I^-$ and $Br^-$) migrate toward Pt (b). As clearly shown in Figure 2, the charge accumulation still exists after removing the electric field, forming a remanent field. Such polarization-induced remanent potential modulates the $I_{light}$ of PDs by modifying the SBH. The positive remanent potential on the source (Pt (a)) side due to accumulation of cations decreased the SBH ($\Phi_{2a} < \Phi_a$), as shown in Figure 5b. This effect could increase the electron injection into the SCs, leading to a higher $I_{light}$. Conversely, the $I_{light}$ of both PDs suppressed after +5 V polarization due to the negative remanent potential on the source (Pt (a)) formed by anions accumulation. This effect increases the SBH ($\Phi_a < \Phi_{3a}$) and repels the electrons near the Pt-SC interface (Figure 5c). The higher order of ion migration in the $MAPbI_3$ than $MAPb(I_{0.88}Br_{0.12})_3$ SCs leads to higher polarization induced remanent potential. Therefore, the $I_{light}$ of $MAPbI_3$ SC-based PDs is highly affected by polarization. In addition, when the PD is under operating voltage, the Fermi levels of perovskite and the Pt electrode are shifted, as seen in Figure 5d. During the forward poling, the cations in the SC move along the polarization field direction and accumulate near the source. This process decreases the SBH ($\Phi_{5a} < \Phi_{4a}$) and increases the electron injection into the SCs leading to a higher $I_{light}$ (Figure 5e). On the other hand, SBH increases under reverse polarization due to anions accumulation near the source, thereby causing $I_{light}$ losses (Figure 5f).

## 4. CONCLUSIONS

In summary, the effect of polarization on the photodetection properties of SC-based PDs based on $MAPbI_3$ and $MAPb(I_{0.88}Br_{0.12})_3$ perovskites has been investigated through systematic experiments. Under dark conditions, the current significantly increases with increasing time and saturates at a higher value of time due to the slow response of mobile ions inside the SCs. The PD based on $MAPb(I_{0.88}Br_{0.12})_3$ SC takes a higher time to saturate the dark current and lowers the difference between $I_0$ and $I_s$ for every applied bias other than the $MAPbI_3$ SC. It was attributed to the reduced size of the unit cell and higher activation energy of the $MAPb(I_{0.88}Br_{0.12})_3$ SC (cubic) than the $MAPbI_3$ SC (tetragonal), which slow down the cation dynamic and movement of mobile ions. Moreover, the presence of remanent current in both PDs after


https://doi.org/10.1021/acs.jpcc.2c03735
J. Phys. Chem. C 2022, 126, 13458−13466

polarization confirms the accumulation of the opposite mobile ions nearby the electrode. The polarization-induced impedance behavior of the $MAPbI_3$ SC denied the possibility of change in electronic doping by the dynamic mobile ions. By capitalizing of the poling-induced ion accumulation on the photodetectivity of both PDs, we found that the change of $I_{light}$ is greater in the $MAPbI_3$ than $MAPb(I_{0.88}Br_{0.12})_3$ SC-based PDs due to the higher ion accumulation in $MAPbI_3$ SC nearby metal electrodes. Our results also showed that the poling-induced remanent potential in the area of Schottky junctions can modify the interface band bending and control the electron injection into the SCs. As a result, adjustable SBH leads to a tunable $I_{light}$ in the investigated SC-based PDs. Understanding the relationship between perovskite crystal structure and polarization-induced ion migration on the photodetection properties in SC-based PDs will help to further optimize the performance of perovskite-based optoelectronic devices.

## ■ ASSOCIATED CONTENT

### Supporting Information

The Supporting Information is available free of charge at https://pubs.acs.org/doi/10.1021/acs.jpcc.2c03735.

pXRD pattern, dark current at different times as a function of applied bias, remanent negative current, Nyquist plots, photocurrent vs illumination power densities, dark $I-V$ curve, current−time curves (PDF)

## ■ AUTHOR INFORMATION


### Corresponding Authors

**Daniel Prochowicz** − *Institute of Physical Chemistry, Polish Academy of Sciences, Warsaw 01-224, Poland;* orcid.org/0000-0002-5003-5637; Email: dprochowicz@ichf.edu.pl

**Apurba Mahapatra** − *Institute of Physical Chemistry, Polish Academy of Sciences, Warsaw 01-224, Poland;* Email: amahapatra@ichf.edu.pl

### Authors

**Rohit D. Chavan** − *Institute of Physical Chemistry, Polish Academy of Sciences, Warsaw 01-224, Poland*

**Mohammad Mahdi Tavakoli** − *Department of Electrical Engineering and Computer Science, Massachusetts Institute of Technology, Cambridge, Massachusetts 02139, United States;* orcid.org/0000-0002-8393-6028

**Pawan Kumar** − *Department of Physics & Astronomy, National Institute of Technology, Rourkela 769008, India*

**Abul Kalam** − *Department of Chemistry, Faculty of Science, King Khalid University, Abha 61413, Saudi Arabia*

**Pankaj Yadav** − *Department of Solar Energy, School of Technology, Pandit Deendayal Energy University, Gandhinagar, Gujarat 382 007, India;* orcid.org/0000-0002-1858-8397

Complete contact information is available at: https://pubs.acs.org/10.1021/acs.jpcc.2c03735


### Notes

The authors declare no competing financial interest.

## ■ ACKNOWLEDGMENTS

A.M. and D.P. acknowledge the National Science Centre (Grant OPUS-20, No. 2020/39/B/ST5/01497) for financial support. A.K. thanks the Dean of Scientific Research, King Khalid University for financial support by Grant No. RGP2/188/43. P.Y. acknowledges the Polish National Agency for Academic Exchange program (PPN/ULM/2020/1/00048).

## ■ REFERENCES


(1) Kojima, A.; Teshima, K.; Shirai, Y.; Miyasaka, T. Organometal Halide Perovskites as Visible-Light Sensitizers for Photovoltaic Cells. *J. Am. Chem. Soc.* **2009**, *131*, 6050−6051.

(2) Jena, A. K.; Kulkarni, A.; Miyasaka, T. Halide Perovskite Photovoltaics: Background, Status, and Future Prospects. *Chem. Rev.* **2019**, *119*, 3036−3103.

(3) Chouhan, L.; Ghimire, S.; Subrahmanyam, C.; Miyasaka, T.; Biju, V. Synthesis, Optoelectronic Properties and Applications of Halide Perovskites. *Chem. Soc. Rev.* **2020**, *49*, 2869−2885.

(4) Li, C.; Huang, W.; Gao, L.; Wang, H.; Hu, L.; Chen, T.; Zhang, H. Recent Advances in Solution-Processed Photodetectors Based on Inorganic and Hybrid Photo-Active Materials. *Nanoscale* **2020**, *12*, 2201−2227.

(5) Wang, J.; Zardetto, V.; Datta, K.; Zhang, D.; Wienk, M. M.; Janssen, R. A. J. 16.8% Monolithic All-Perovskite Triple-Junction Solar Cells via a Universal Two-Step Solution Process. *Nat. Commun.* **2020**, *11*, 1−10.

(6) Sahare, S.; Pham, H. D.; Angmo, D.; Ghoderao, P.; MacLeod, J.; Khan, S. B.; Lee, S. L.; Singh, S. P.; Sonar, P. Emerging Perovskite Solar Cell Technology: Remedial Actions for the Foremost Challenges. *Adv. Energy Mater.* **2021**, *11*, 2101085.

(7) Tavakoli, M. M.; Dastjerdi, H. T.; Yadav, P.; Prochowicz, D.; Si, H.; Tavakoli, R. Ambient Stable and Efficient Monolithic Tandem Perovskite/PbS Quantum Dots Solar Cells via Surface Passivation and Light Management Strategies. *Adv. Funct. Mater.* **2021**, *31*, 2010623.

(8) Lin, K.; Xing, J.; Quan, L. N.; de Arquer, F. P. G.; Gong, X.; Lu, J.; Xie, L.; Zhao, W.; Zhang, D.; Yan, C.; Li, W.; Liu, X.; Lu, Y.; Kirman, J.; Sargent, E. H.; Xiong, Q.; Wei, Z. Perovskite Light-Emitting Diodes with External Quantum Efficiency Exceeding 20 per Cent. *Nature* **2018**, *562*, 245−248.

(9) Van Le, Q.; Jang, H. W.; Kim, S. Y. Recent Advances toward High-Efficiency Halide Perovskite Light-Emitting Diodes: Review and Perspective. *Small Methods* **2018**, *2*, 1700419.

(10) Liu, Y.; Chen, P.-A.; Hu, Y. Recent Developments in Fabrication and Performance of Metal Halide Perovskite Field-Effect Transistors. *J. Mater. Chem. C* **2020**, *8*, 16691−16715.

(11) Meloni, S.; Moehl, T.; Tress, W.; Franckeviius, M.; Saliba, M.; Lee, Y. H.; Gao, P.; Nazeeruddin, M. K.; Zakeeruddin, S. M.; Rothlisberger, U.; Graetzel, M. Ionic Polarization-Induced Current−Voltage Hysteresis in $CH_3NH_3PbX_3$ Perovskite Solar Cells. *Nat. Commun.* **2016**, *7*, 10334.

(12) Liu, P.; Wang, W.; Liu, S.; Yang, H.; Shao, Z. Fundamental Understanding of Photocurrent Hysteresis in Perovskite Solar Cells. *Adv. Energy Mater.* **2019**, *9*, 1803017.

(13) Lan, C.; Zou, H.; Wang, L.; Zhang, M.; Pan, S.; Ma, Y.; Qiu, Y.; Lin Wang, Z.; Lin, Z. Revealing Electrical-Poling-Induced Polarization Potential in Hybrid Perovskite Photodetectors. *Adv. Mater.* **2020**, *32*, 2005481.

(14) Wang, H.; Guerrero, A.; Bou, A.; Al-Mayouf, A. M.; Bisquert, J. Kinetic and Material Properties of Interfaces Governing Slow Response and Long Timescale Phenomena in Perovskite Solar Cells. *Energy Environ. Sci.* **2019**, *12*, 2054−2079.

(15) Cho, Y.; Jung, H. R.; Jo, W. Photo-Induced Defects in $MAPbBr_3$ Single Crystals. *J. Phys. Energy* **2021**, *3*, No. 044005.

(16) Bischak, C. G.; Hetherington, C. L.; Wu, H.; Aloni, S.; Ogletree, D. F.; Limmer, D. T.; Ginsberg, N. S. Origin of Reversible Photoinduced Phase Separation in Hybrid Perovskites. *Nano Lett.* **2017**, *17*, 1028−1033.

(17) Mahapatra, A.; Parikh, N.; Kumar, P.; Kumar, M.; Prochowicz, D.; Kalam, A.; Tavakoli, M. M.; Yadav, P. Changes in the Electrical Characteristics of Perovskite Solar Cells with Aging Time. *Molecules* **2020**, *25*, 2299.

(18) Chen, B.; Rudd, P. N.; Yang, S.; Yuan, Y.; Huang, J. Imperfections and Their Passivation in Halide Perovskite Solar Cells. *Chem. Soc. Rev.* **2019**, *48*, 3842−3867.

(19) Phung, N.; Al-Ashouri, A.; Meloni, S.; Mattoni, A.; Albrecht, S.; Unger, E. L.; Merdasa, A.; Abate, A. The Role of Grain Boundaries on Ionic Defect Migration in Metal Halide Perovskites. *Adv. Energy Mater.* **2020**, *10*, 1903735.
(20) Mahapatra, A.; Prochowicz, D.; Tavakoli, M. M.; Trivedi, S.; Kumar, P.; Yadav, P. A Review of Aspects of Additive Engineering in Perovskite Solar Cells. *J. Mater. Chem. A* **2020**, *8*, 27−54.
(21) Trivedi, S.; Prochowicz, D.; Parikh, N.; Mahapatra, A.; Pandey, M. K.; Kalam, A.; Tavakoli, M. M.; Yadav, P. Recent Progress in Growth of Single-Crystal Perovskites for Photovoltaic Applications. *ACS Omega* **2021**, *6*, 1030−1042.
(22) Li, J.; Han, Z.; Gu, Y.; Yu, D.; Liu, J.; Hu, D.; Xu, X.; Zeng, H. Perovskite Single Crystals: Synthesis, Optoelectronic Properties, and Application. *Adv. Funct. Mater.* **2021**, *31*, 2008684.
(23) Miao, J.; Zhang, F. Recent Progress on Highly Sensitive Perovskite Photodetectors. *J. Mater. Chem. C* **2019**, *7*, 1741−1791.
(24) Leijtens, T.; Hoke, E. T.; Grancini, G.; Slotcavage, D. J.; Eperon, G. E.; Ball, J. M.; De Bastiani, M.; Bowring, A. R.; Martino, N.; Wojciechowski, K.; McGehee, M. D.; Snaith, H. J.; Petrozza, A. Mapping Electric Field-Induced Switchable Poling and Structural Degradation in Hybrid Lead Halide Perovskite Thin Films. *Adv. Energy Mater.* **2015**, *5*, 1500962.
(25) Xiao, Z.; Yuan, Y.; Shao, Y.; Wang, Q.; Dong, Q.; Bi, C.; Sharma, P.; Gruverman, A.; Huang, J. Giant Switchable Photovoltaic Effect in Organometal Trihalide Perovskite Devices. *Nat. Mater.* **2015**, *14*, 193−198.
(26) García-Batlle, M.; Baussens, O.; Amari, S.; Zaccaro, J.; Gros-Daillon, E.; Verilhac, J. M.; Guerrero, A.; Garcia-Belmonte, G. Moving Ions Vary Electronic Conductivity in Lead Bromide Perovskite Single Crystals through Dynamic Doping. *Adv. Electron. Mater.* **2020**, *6*, 2000485.
(27) Wang, X.-Y.; Wang, H.; Chen, L.-R.; Shao, Y.-C.; Shao, J.-D. Suppression of Ion Migration in Perovskite Materials by Pulse-Voltage Method. *Chinese Phys. B* **2021**, *30*, 118104.
(28) Bruno, A.; Cortecchia, D.; Yu Chin, X.; Fu, K.; Boix, P. P.; Mhaisalkar, S.; Soci, C. Temperature and Electrical Poling Effects on Ionic Motion in $MAPbI_3$ Photovoltaic Cells. *Adv. Energy Mater.* **2017**, *7*, 1700265.
(29) Zou, Y.; Holmes, R. J. Temperature-Dependent Bias Poling and Hysteresis in Planar Organo-Metal Halide Perovskite Photovoltaic Cells. *Adv. Energy Mater.* **2016**, *6*, 1501994.
(30) Yuan, Y.; Wang, Q.; Shao, Y.; Lu, H.; Li, T.; Gruverman, A.; Huang, J. Electric-Field-Driven Reversible Conversion Between Methylammonium Lead Triiodide Perovskites and Lead Iodide at Elevated Temperatures. *Adv. Energy Mater.* **2016**, *6*, 1501803.
(31) Moia, D.; Gelmetti, I.; Calado, P.; Fisher, W.; Stringer, M.; Game, O.; Hu, Y.; Docampo, P.; Lidzey, D.; Palomares, E.; Nelson, J.; Barnes, P. R. F. Ionic-to-Electronic Current Amplification in Hybrid Perovskite Solar Cells: Ionically Gated Transistor-Interface Circuit Model Explains Hysteresis and Impedance of Mixed Conducting Devices. *Energy Environ. Sci.* **2019**, *12*, 1296−1308.
(32) Yuan, Y.; Li, T.; Wang, Q.; Xing, J.; Gruverman, A.; Huang, J. Anomalous Photovoltaic Effect in Organic-Inorganic Hybrid Perovskite Solar Cells. *Sci. Adv.* **2017**, *3*, No. e1602164.
(33) Lian, Z.; Yan, Q.; Lv, Q.; Wang, Y.; Liu, L.; Zhang, L.; Pan, S.; Li, Q.; Wang, L.; Sun, J.-L. High-Performance Planar-Type Photodetector on (100) Facet of $MAPbI_3$ Single Crystal. *Sci. Rep.* **2015**, *5*, 16563.
(34) Mahapatra, A.; Prochowicz, D.; Kruszyńska, J.; Satapathi, S.; Akin, S.; Kumari, H.; Kumar, P.; Fazel, Z.; Tavakoli, M. M.; Yadav, P. Effect of Bromine Doping on the Charge Transfer, Ion Migration and Stability of the Single Crystalline $MAPb(Br_xI_{1-x})_3$ Photodetector. *J. Mater. Chem. C* **2021**, *9*, 15189−15200.
(35) Zou, H.; Li, X.; Peng, W.; Wu, W.; Yu, R.; Wu, C.; Ding, W.; Hu, F.; Liu, R.; Zi, Y.; Lin Wang, Z. Piezo-Phototronic Effect on Selective Electron or Hole Transport through Depletion Region of Vis−NIR Broadband Photodiode. *Adv. Mater.* **2017**, *29*, 1701412.
(36) Shrestha, S.; Tsai, H.; Yoho, M.; Ghosh, D.; Liu, F.; Lei, Y.; Tisdale, J.; Baldwin, J.; Xu, S.; Neukirch, A. J.; Tretiak, S.; Vo, D.; Nie, W. Role of the Metal-Semiconductor Interface in Halide Perovskite Devices for Radiation Photon Counting. *ACS Appl. Mater. Interfaces* **2020**, *12*, 45533−45540.
(37) Lai, Q.; Zhu, L.; Pang, Y.; Xu, L.; Chen, J.; Ren, Z.; Luo, J.; Wang, L.; Chen, L.; Han, K.; Lin, P.; Li, D.; Lin, S.; Chen, B.; Pan, C.; Wang, Z. L. Piezo-Phototronic Effect Enhanced Photodetector Based on $CH_3NH_3PbI_3$ Single Crystals. *ACS Nano* **2018**, *10*, 10501−10508.
(38) Lin, P.; Meng, Q.; Chen, H.; Hu, H.; Fang, D.; Xu, L.; Wang, P.; Cui, C. Variational Hysteresis and Photoresponse Behavior of $MAPbX_3$ (X = I, Br, Cl) Perovskite Single Crystals. *J. Phys.: Condens. Matter* **2021**, *33*, 285703.
(39) Kalam, A.; Runjhun, R.; Mahapatra, A.; Tavakoli, M. M.; Trivedi, S.; Tavakoli Dastjerdi, H.; Kumar, P.; Lewiński, J.; Pandey, M. K.; Prochowicz, D.; Yadav, P. Interpretation of Resistance, Capacitance, Defect Density, and Activation Energy Levels in Single-Crystalline $MAPbI_3$. *J. Phys. Chem. C* **2020**, *124* (6), 3496−3502.
(40) Mahapatra, A.; Runjhun, R.; Nawrocki, J.; Lewiński, J.; Kalam, A.; Kumar, P.; Trivedi, S.; Tavakoli, M. M.; Prochowicz, D.; Yadav, P. Elucidation of the Role of Guanidinium Incorporation in Single-Crystalline $MAPbI_3$ Perovskite on Ion Migration and Activation Energy. *Phys. Chem. Chem. Phys.* **2020**, *22*, 11467−11473.
(41) Liu, Y.; Borodinov, N.; Lorenz, M.; Ahmadi, M.; Kalinin, S. V.; Ievlev, A. V.; Ovchinnikova, O. S. Hysteretic Ion Migration and Remanent Field in Metal Halide Perovskites. *Adv. Sci.* **2020**, *7*, 2001176.
(42) Li, C.; Guerrero, A.; Huettner, S.; Bisquert, J. Unravelling the Role of Vacancies in Lead Halide Perovskite through Electrical Switching of Photoluminescence. *Nat. Commun.* **2018**, *9*, 5113.
(43) de la Barrera, S. C.; Cao, Q.; Gao, Y.; Gao, Y.; Bheemarasetty, V. S.; Yan, J.; Mandrus, D. G.; Zhu, W.; Xiao, D.; Hunt, B. M. Direct Measurement of Ferroelectric Polarization in a Tunable Semimetal. *Nat. Commun.* **2021**, *12*, 5298.
(44) Chen, X.; German, L.; Bong, J.; Yu, Y.; Starr, M.; Qin, Y.; Ma, Z.; Wang, X. Decoupling the Charge Collecting and Screening Effects in Piezotronics-Regulated Photoelectrochemical Systems by Using Graphene as the Charge Collector. *Nano Energy* **2018**, *48*, 377−382.
(45) Li, H.; Li, F.; Shen, Z.; Han, S. T.; Chen, J.; Dong, C.; Chen, C.; Zhou, Y.; Wang, M. Photoferroelectric Perovskite Solar Cells: Principles. *Advances and Insights. Nano Today* **2021**, *37*, 101062.
(46) Beilsten-Edmands, J.; Eperon, G. E.; Johnson, R. D.; Snaith, H. J.; Radaelli, P. G. Non-Ferroelectric Nature of the Conductance Hysteresis in $CH_3NH_3PbI_3$ Perovskite-Based Photovoltaic Devices. *Appl. Phys. Lett.* **2015**, *106*, 173502.
(47) Nandi, P.; Topwal, D.; Park, N. G.; Shin, H. Organic-Inorganic Hybrid Lead Halides as Absorbers in Perovskite Solar Cells: A Debate on Ferroelectricity. *J. Phys. D. Appl. Phys.* **2020**, *53*, 493002.
(48) Li, W.; Man, Z.; Zeng, J.; Zheng, L.; Zeng, H.; Zhao, K.; Li, G.; Kassiba, A. Poling Effect on the Electrostrictive and Piezoelectric Response in $CH_3NH_3PbI_3$ Single Crystals. *Appl. Phys. Lett.* **2021**, *118*, 151905.
(49) Shahrokhi, S.; Gao, W.; Wang, Y.; Anandan, P. R.; Rahaman, M. Z.; Singh, S.; Wang, D.; Cazorla, C.; Yuan, G.; Liu, J. M.; Wu, T. Emergence of Ferroelectricity in Halide Perovskites. *Small Methods* **2020**, *4*, 2000149.


https://doi.org/10.1021/acs.jpcc.2c03735
J. Phys. Chem. C 2022, 126, 13458−13466